

Simulation optimized design of graphene-based hybrid plasmonic waveguide

A Asadi¹, M R Jafari^{2*}  and M Shahmansouri¹

¹Department of Physics, Faculty of Science, Arak University, Arak 3815688349, Iran

²Department of Condensed Matter Physics, Faculty of Physics, Alzahra University, Tehran 1993891167, Iran

Received: 17 February 2022 / Accepted: 10 January 2023 / Published online: 30 January 2023

Abstract: A unique graphene-based hybrid plasmonic waveguide (GHPW) is proposed with a relatively high figure of merit (FOM) and long propagation length (L_{spp}) in the far-infrared (FIR) region. The proposed waveguide is combined of a high-index cylindrical dielectric in the coordinate origin, a low-index dielectric strip, and a monolayer graphene that set are surrounded by SiO₂ rectangular cube. The modal features of the graphene surface plasmon polariton (SPP) mode are investigated via the finite element technique. Finding results display that a propagation length of $\sim 10^5$ nm and a figure of merit $\sim 10^5$ can be obtained by tuning the dimensions of the waveguide geometry and the different materials. Therefore, propagation properties of the proposed waveguide improve significantly by changing the materials type of dielectric strip and cylindrical dielectric. According to the present findings, the GHPW can be used in the optoelectronic and photonic devices.

Keywords: Graphene; Plasmonic; Waveguide; Propagation length

1. Introduction

The surface plasmon polaritons (SPPs) are collective electron oscillations coupled to a light field which propagate along the dielectric-metal interface [1]. The surface plasmon phenomenon in the nano-micro structures results in excellent consequences within the domains of filter [2], surface-enhanced Raman [3], waveguides [4], sensors [5], lithography [6], etc. [7–9]. The SPPs can guide light at scales very shorter than the diffraction limit in the far-infrared (FIR) range [10]. SPPs in the far-infrared (FIR) range or terahertz frequencies have very longer propagation length and lower loss compared with the visible spectral range [10]. The plasmonic waveguides guide electromagnetic waves with less loss of energy and are utilized as ingredients in optical integrated circuits or as optical communication. Metal-based hybrid plasmonic waveguides (MHPW) are mighty of guiding electromagnetic waves with subwavelength confinement smaller than the diffraction limit [11] compared to the dielectric-based waveguides including silicon-on-glass waveguides [12],

photonic crystal fibers [13], and slab waveguides [14]. Therefore, in order to enhance the surface Plasmon-polaritons propagation distance, various types of MHPW as wedged, channeled [15], and metal gap plasmonic waveguides [16, 17] have been studied. It has been shown that the surface plasmon polaritons guided by MHPW can attain the normalized mode area of $\sim 10^{-3} - 1$ and long propagation length of $\sim 0.01 - 100$ mm at the wavelength of $1.55\mu\text{m}$ [18, 19]. Nevertheless, immediately expanding the waveguide design in the terahertz frequency will direct to a considerable decay in the subwavelength confinement, making it inappropriate for compact integration [20]. Therefore, by utilizing dielectric materials without the electrostatic adjustability's, like noble metals, all fore-named waveguides suffer from the intrinsic defect not tunable once the waveguides are fixed after construction [21, 22].

Graphene, as a nanomaterial developed two-dimensional (2D) material, has been a matter of interest in nano-photonics and optoelectronics [23–26]. Due to supporting SPPs in the infrared spectrum, graphene is noticed as one of the most plasmonic materials premieres to noble metals with higher mode confinement, comparatively long propagation distance, particularly with important excellence of being

*Corresponding author, E-mail: mo.jafari@alzahra.ac.ir

tunable through electrostatic doping or chemical doping [27–29]. Because of these unique properties, the waveguiding characteristics of graphene surface plasmon polaritons (GSPPs) have been considered extensively in the various structures [30–32]. Because of these interesting specifications, graphene is studied as an appropriate material for the future compact hybrid plasmonic waveguide applications. During the last years, a number of authors have investigated regarding graphene-based adjustable plasmonic systems consisting modulators [32], switches [33], waveguides [34], absorbers [35], biosensors [36], etc. This study intends to suggest a new graphene-based hybrid plasmonic waveguide (GHPW), which is composed of a high-index cylindrical dielectric in the coordinate origin, a low-index dielectric strip, and a monolayer graphene that set are surrounded by SiO₂ rectangular cube. Advantage of the GHPW structure is longer propagation length in comparison with the traditional graphene plasmonic waveguides, (see references [10, 37]). In the present study, we proposed a new structure to optimum the propagation properties of GHPW. Then, the effects of the physical parameters (geometry and material) of the high-index cylindrical dielectric and low-index dielectric strip on the guiding features of the proposed structures are studied. It can be theoretically revealed that not only through the type of materials but also through the key structural parameters, tuning of the high-index cylindrical dielectric and low-index dielectric strip, the proposed structure can be utilized as a high-performance GHPW in the range of FIR spectral.

2. Mathematical formulation

Figure 1 represents the schematic configuration of the suggested waveguide, constituting a high-index cylindrical

dielectric in the coordinate origin, a low-index dielectric strip, and a monolayer graphene that set are surrounded by SiO₂ rectangular cube. The proposed structure includes some important physical parameters involving the thickness t of dielectric strip, and radius R of the cylinder, that play role of control parameters. We consider the plasmonic properties dependence of the proposed GHPW for different materials of the dielectric strip when the strip thickness varies from 1 to 5 μm . Here, MgF₂, KCL, SiO₂, and the high-density polyethylene (HDPE) materials with the relative permittivities of 1.7, 2.13, 2.25, and 2.37, have been used for dielectric strip, respectively [10, 38–40]. In addition, we study the dependency of the plasmonic features of the proposed waveguide for the various high-index cylindrical dielectric materials, when the radius of the cylinder varies from 5 to 15 μm . We have used InSb, Ge, GaSb, and GaAs with the relative permittivity of 16.8, 16.2, 15.7, and 12.25, respectively [10, 27, 41–44].

Graphene has been proved to be efficiently regarded as a 2D surface conductivity σ_g in various graphene-based device simulations [45–47]. Hence, the graphene is modeled, in this paper, as a 2D surface conductivity σ_g in the simulation. In the far-infrared spectrum, the calculation of σ_g for the graphene sheet is conducted via the Kubo equation with terms of the intraband and interband [32, 48], as follows:

$$\sigma_g(\omega, \mu_c, \Gamma, T) = \sigma_{\text{intra}}(\omega, \mu_c, \Gamma, T) + \sigma_{\text{inter}}(\omega, \mu_c, \Gamma, T) \quad (1)$$

$$\sigma_{\text{intra}}(\omega, \mu_c, \Gamma, T) = \frac{je^2}{\pi\hbar^2(\omega - j2\Gamma)} \int_0^\infty \left(\frac{\partial f_d(\xi, \mu_c, T)}{\partial \xi} - \frac{\partial f_d(-\xi, \mu_c, T)}{\partial \xi} \right) \xi d\xi \quad (2)$$

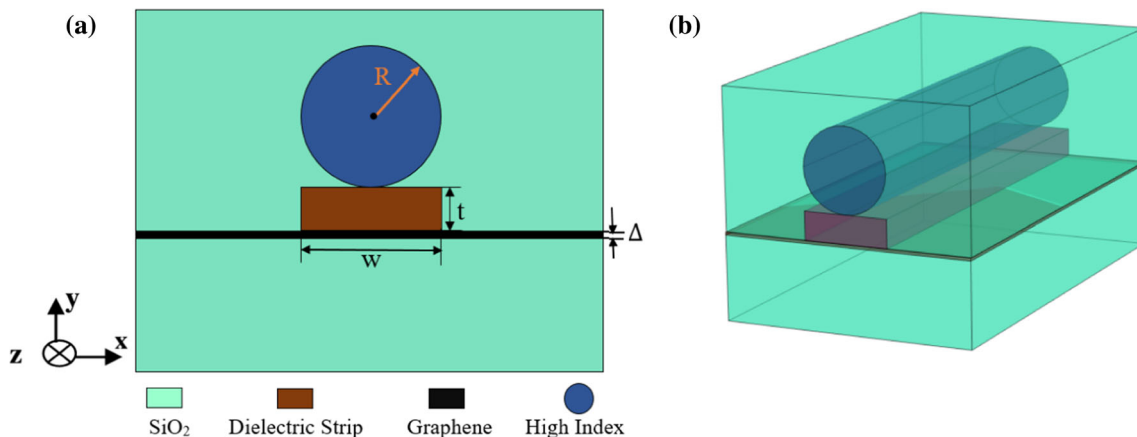


Fig. 1 Schematic configuration of proposed graphene-based hybrid plasmonic waveguide (a) cross section of the waveguide. (b) 3D structure of the waveguide

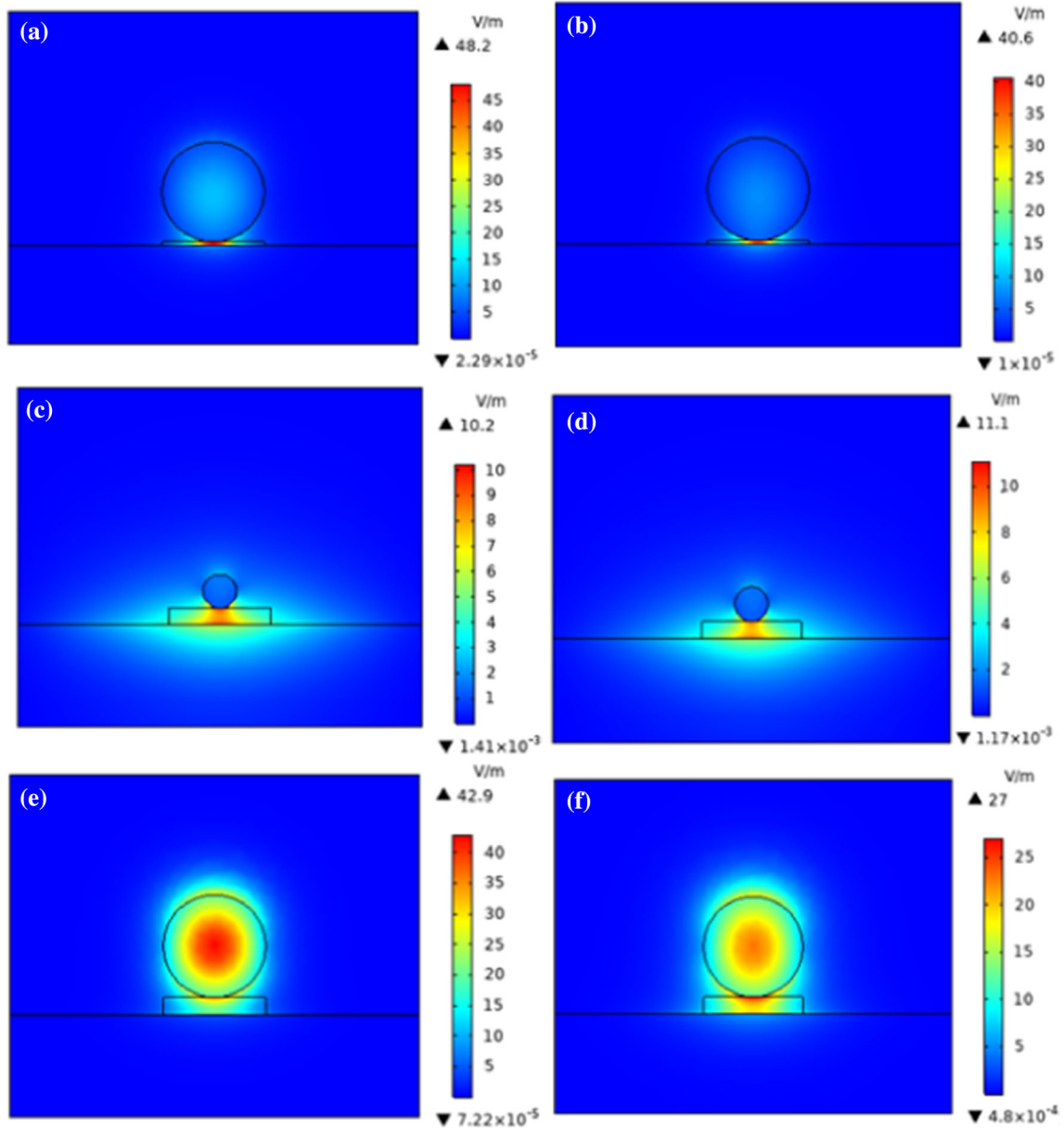


Fig. 2 The electric field distributions of the GHPW with different materials and dimensions of GHPW that reported in Table 1

$$\sigma_{\text{inter}}(\omega, \mu_c, \Gamma, T) = \frac{-je^2(\omega - j2\Gamma)}{\pi\hbar^2} \int_0^\infty \left(\frac{f_d(-\xi, \mu_c, T) - f_d(\xi, \mu_c, T)}{(\omega - j2\Gamma)^2 - 4\left(\frac{\xi}{\hbar}\right)^2} \right) d\xi \quad (3)$$

where

$$f_d(\xi, \mu_c, T) = \frac{1}{e^{(\xi - \mu_c)/k_B T} + 1} \quad (4)$$

where ω , μ_c , Γ and T are the angular frequency, the chemical potential or Fermi energy, the scattering rate with $\Gamma = 2/\tau$, and the temperature, respectively. The symbol τ is the relaxation time, which is determined by the carrier mobility μ in the graphene. Also, e , ξ , \hbar , k_B , and

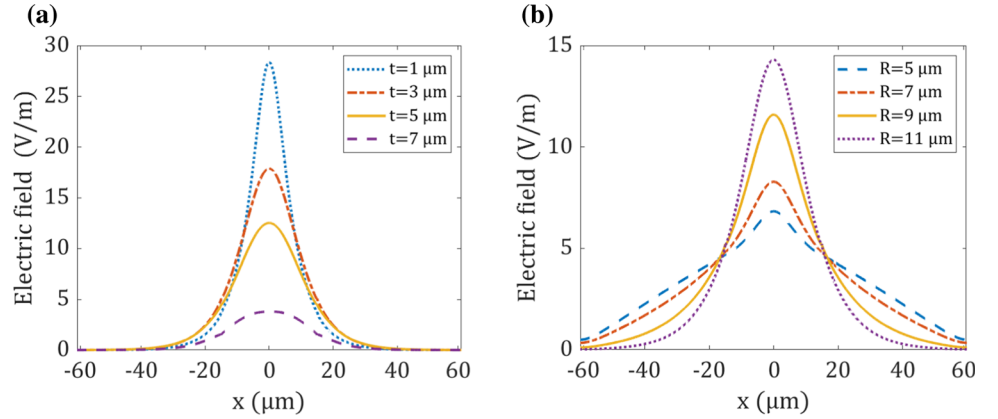
$f_d(\xi, \mu_c, T)$ are the electron charge, the energy, the reduced Plank constant, the Boltzmann constant and the Fermi–Dirac distribution function, respectively. In this study, we set the parameter values as follows: the temperature $T = 300$ K, $\mu_c = 0.5$ eV, the frequency $f = 3$ THz, the relaxation time $\tau = 0.5$ ps and the Fermi velocity $v_F = 10^6$ m/s[49]. The graphene dielectric constant can be measured as in [10]

$$\epsilon_g = 1 + \frac{i\sigma_g\eta_0}{k_0\Delta} \quad (5)$$

where η_0 is air impedance, k_0 is the wave number, and $\Delta = 0.5$ nm is the graphene layer thickness. The key

Table 1 The numerical parameter values of different materials and dimensions according to the electric field distributions illustrated in Fig. 2

Figure	The high-index cylindrical dielectric	The low-index dielectric strip	R (μm)	t (μm)	Max (electric field, V/m)
2(a)	InSb	MgF ₂	15	1	48.2
2(b)	InSb	HDPE	15	1	40.6
2(c)	InSb	KCl	5	5	10.2
2(d)	InSb	SiO ₂	5	5	11.1
2(e)	GaSb	MgF ₂	15	5	42.9
2(f)	GaAs	MgF ₂	15	5	27

Fig. 3 The electric field distributions along the x-axis for (a) $R = 15\mu\text{m}$ and different strip thickness. (b) $t = 5\mu\text{m}$, and different cylinder radius

plasmonic parameters can be calculated through the changes in physical dimensions and materials. Thus, the effective refractive index for the proposed waveguide can be defined as [50]

$$N_{\text{eff}} = \frac{k_z}{k_0} \quad (6)$$

where k_z is the z-component of the constant of propagation. The propagation length of SPPs mode can be defined [32]

$$L_{\text{spp}} = \frac{\lambda_0}{4\pi \text{Im}(N_{\text{eff}})} \quad (7)$$

where λ_0 is the wavelength in free space. As to the comparison of the optical devices performances of various configurations, the definition of figure of merit (FOM) can be obtained as [32]

$$\text{FOM} = \frac{\text{Re}(N_{\text{eff}})}{\text{Im}(N_{\text{eff}})} \quad (8)$$

which will be discussed in the next section.

3. Results and discussion

First, we exhibit the electric field distributions for the hybrid plasmonic mode with TM polarization for different values of radius R of the high-index dielectric cylinder and

the thickness t of the low-index dielectric strip in Fig. 2. The physical parameters used in Fig. 2 are included in Table. 1. The strongest confinement of electric field distribution for the higher values of cylinder radius R and small strip thickness t ($[R, t] = [15\mu\text{m}, 1\mu\text{m}]$) into the strip region is shown in Fig. 2(a) and 2(b). It can be seen that the limited field in the strip region, for MgF₂ (Fig. 2(a)) is greater than that of HDPE (Fig. 2(b)). For the smaller values of radius R and higher strip thickness t ($[R, t] = [5\mu\text{m}, 5\mu\text{m}]$), the most electric field would be confined in the strip region, as illustrated in Fig. 2(c) and 2(d). However, for the higher values of R and t ($[R, t] = [15\mu\text{m}, 5\mu\text{m}]$), the electric field distribution confined both in the strip zone and the dielectric cylinder, as demonstrated in Fig. 2(e) and 2(f), but the amount of electric field confinement in the cylindrical dielectric region, for GaSb (Fig. 2(e)), is greater than that of GaAs (Fig. 2(f)).

Figure 3 presents the chart of electric field on the x-axis for the different values of radius R of the high-index dielectric cylinder and the thickness t of the low-index dielectric strip in coordinate of $(x, y) = (x, -R - t)$. Figure 3(a) demonstrates that the electric field couples to the MgF₂ strip in the designed waveguide increases with decreasing the strip thickness from 7 to 1 μm for $R = 15\mu\text{m}$. When $t = 1\mu\text{m}$, the cylinder mode is extremely coupled to the SPP mode, and most of the electric field is focused within the strip region. But, Fig. 3(b) shows that

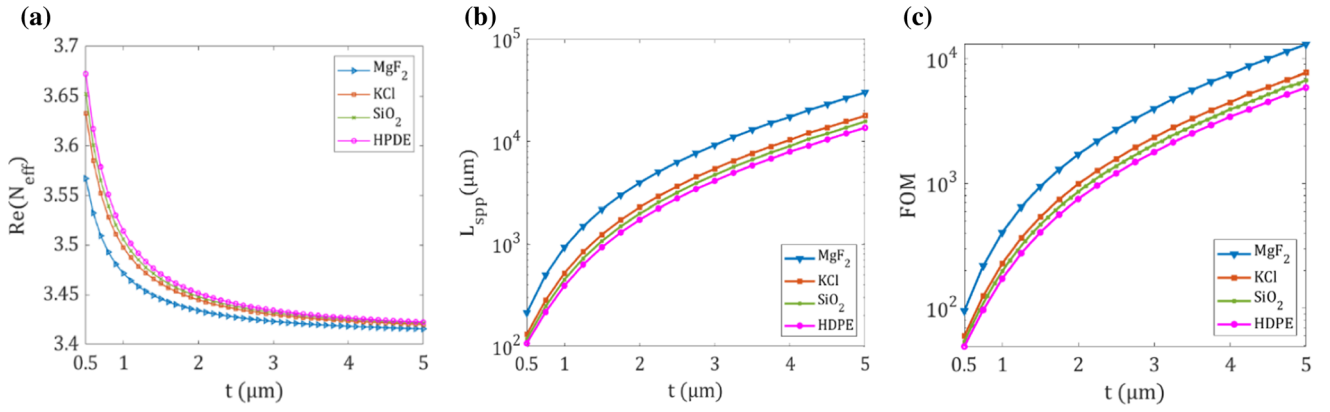


Fig. 4 Dependency of the plasmonic features (a) the $\text{Re}(N_{\text{eff}})$, (b) the L_{spp} , and c the FOM on the dielectric strip thickness t for different materials

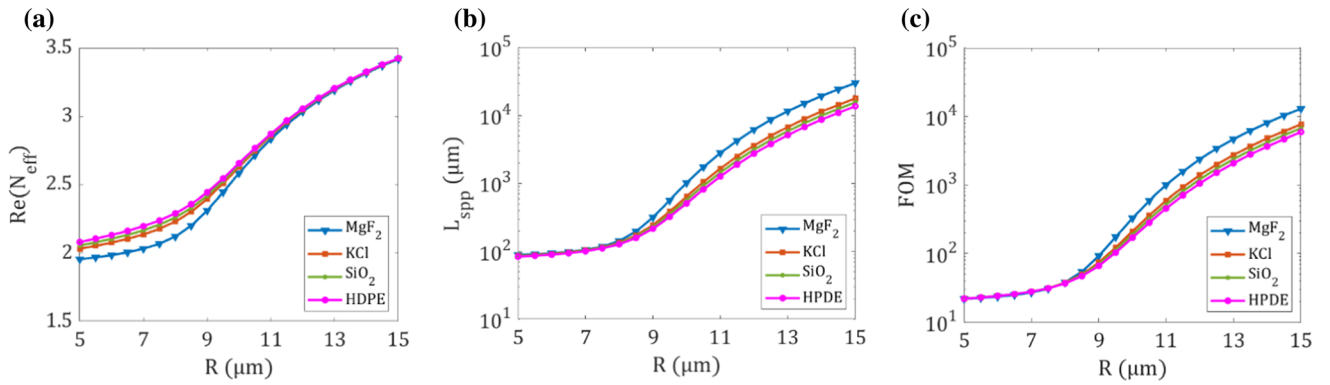


Fig. 5 The plasmonic features as a function of the cylinder radius R (a) $\text{Re}(N_{\text{eff}})$, (b) L_{spp} , and (c) FOM for different dielectric strip materials

by increasing the cylinder radius R from 7 to 11 μm at $t = 1 \mu\text{m}$, the electric field is confined inside the InSb cylinder.

The real part of the effective refractive index ($\text{Re}(N_{\text{eff}})$), propagation length (L_{spp}), and the figure of merit (FOM) of the proposed GHPW for different dielectric strip materials, where the thickness of the strip changes from 0.5 to 5 μm , are illustrated in Fig. 4. The different materials MgF_2 , KCl , SiO_2 , and HDPE have been used as the dielectric strip materials with the relative permittivities of 1.7, 2.13, 2.25, and 2.37, respectively. Here, the high-index dielectric of cylinder is InSb with the relative permittivity of $\epsilon_{\text{InSb}} = 16.8$ and radius of $R = 15 \mu\text{m}$. Figure 4(a) shows the $\text{Re}(N_{\text{eff}})$ dependence on the dielectric strip thickness. It can be seen that the higher dielectric function of strip with smaller thickness has stronger confinement. In addition, $\text{Re}(N_{\text{eff}})$ decreases by increasing the thickness of the strip. Figure 4(b) and 4(c) shows that L_{spp} and FOM increase drastically by increasing the dielectric strip thickness as well as by decreasing the permittivity of the dielectric strip. It can be seen that designed structure is

expected to guide the SPPs mode with low propagation loss.

Therefore, L_{spp} is drastically enhanced for MgF_2 as compared with the other materials. For example, by increasing the thickness of the dielectric strip from 0.5 to 5 μm , the propagation length L_{spp} increases from 49.43 to 5929 μm for HDPE strip and it increases from 211.9 to 30,300 μm for MgF_2 strip [see Fig. 4(b)]. However, figure of merit FOM increases from 49.43 to 5929 for HDPE strip and it increases from 95.04 to 13,010 for MgF_2 strip [see Fig. 4(c)].

To deeply figure out the mode properties of the GHPW, we analyze the real part of the effective refractive index, the figure of merit, and the propagation length for the SPPs mode through the changing of cylinder radius. The real part of the effective refractive index of the suggested waveguide versus the cylinder radius R for dielectric strip with various materials is shown in Fig. 5(a). Here, the materials are similar to those discussed in Fig. 4. We see that there is weaker confinement with the smaller radius R and lower the dielectric function of strip. It can be seen that $\text{Re}(N_{\text{eff}})$ increases by increasing the permittivity of the dielectric

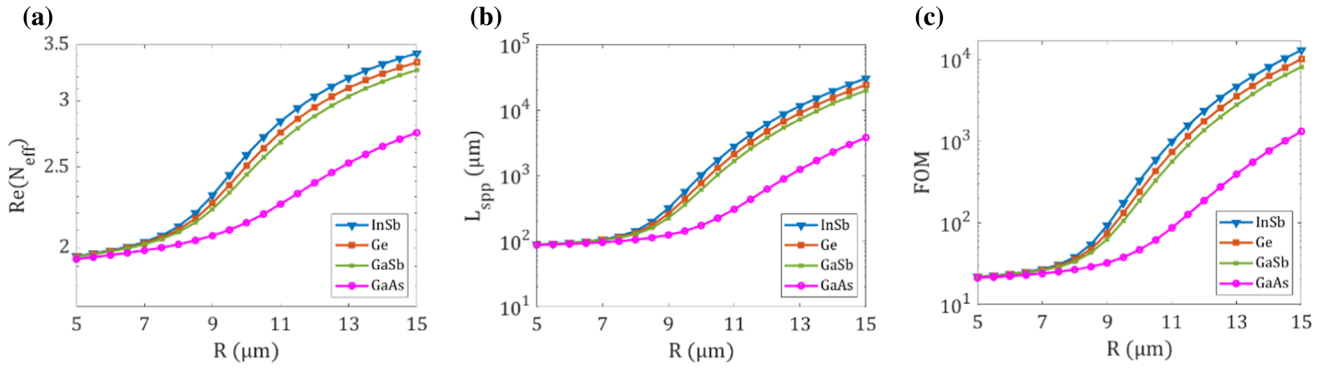


Fig. 6 Diagrams (a–c) present the $\text{Re}(N_{\text{eff}})$, L_{spp} , and FOM as a function of the cylinder radius R for different cylinder materials of InSb, Ge, GaSb and GaAs, respectively, with MgF_2 strip with thickness $t = 5\mu\text{m}$

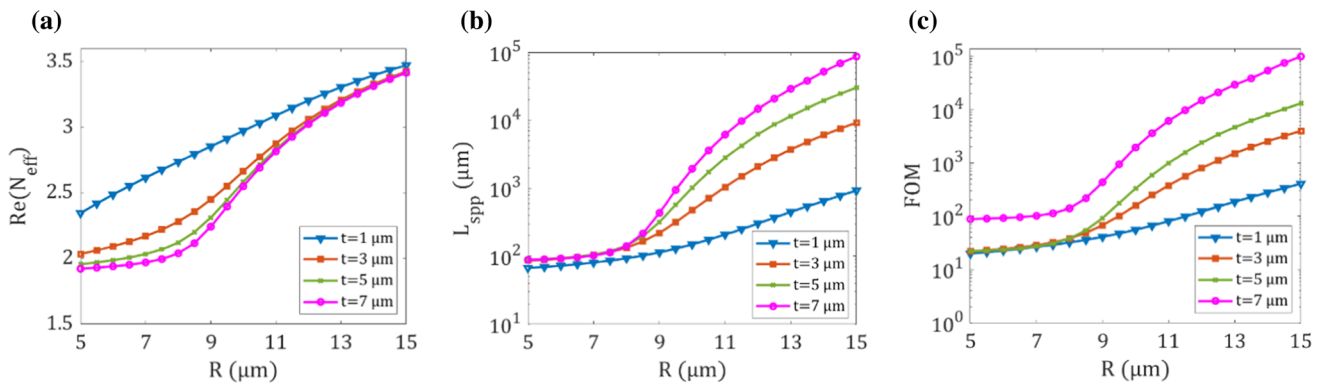


Fig. 7 Dependence of (a) the $\text{Re}(N_{\text{eff}})$, (b) L_{spp} and (c) FOM on radius R of the InSb cylinder for various MgF_2 strips thickness t

strip and radius R . Also, the variation of the $\text{Re}(N_{\text{eff}})$ is similar for all of the dielectric strip materials in the range of $R \geq 12\mu\text{m}$. However, HDPE represents the highest confinement, in $R < 12\mu\text{m}$. Figures 5(b) and 5(c) show that via the increasing values of the radius R , the plasmonic properties of the dielectric strip for each dielectric strip materials remain nearly constant in $R < 8\mu\text{m}$, but in higher radius, by increasing the radius R , the propagation length (L_{spp}) and figure of merit (FOM) increase drastically. Moreover, among the materials used as the dielectric strip, MgF_2 has the highest L_{spp} and FOM. Hence, when a low-index dielectric strip is used (i.e., MgF_2), there is a significant loss reduction that can increase the propagation length.

As to the comprehensive understanding of the propagation features of the designed waveguide, the effect of the cylinder radius R and the dielectric constants of different cylinder materials as InSb, Ge, GaSb and GaAs on the propagation properties are shown in Fig. 6. Figure 6(a)–6(c) presents the dependency of $\text{Re}(N_{\text{eff}})$, L_{spp} , and FOM of the suggested structure on the cylinder various materials of InSb, Ge, GaSb and GaAs, where the relative permittivity is represented as $\epsilon_{\text{InSb}} = 16.8$ and $\epsilon_{\text{Ge}} = 16.2$, $\epsilon_{\text{GaSb}} = 15.7$

and $\epsilon_{\text{GaAs}} = 12.25$. It can be seen that for the fixed values of the relative permittivity, the $\text{Re}(N_{\text{eff}})$, L_{spp} , and FOM increase when the cylinder radius R increases. It can be clarified that the properties of SPP propagation are tuned flexibly through the change in the permittivity of the cylinder. It is observed that the InSb cylinder with higher radius and higher dielectric function shows stronger confinement, longer propagation length, and better figure of merit.

To have an analysis of the geometry parameter's effect on the propagation and mode features, the real part of the effective refractive index, the figure of merit and the propagation length can be considered. Furthermore, for the hybrid mode, these can be taken into consideration via altering the radius R of the InSb cylinder and the MgF_2 strip thickness t . The real part of the effective refractive index of the proposed waveguide compared to the radius of the InSb cylinder for various MgF_2 strip thickness can be represented in Fig. 7. For the fixed value of t , the $\text{Re}(N_{\text{eff}})$ increases when the radius R increases. Figure 7(b) and 7(c) shows the dependences of the propagation length and figure of merit on the radius R of InSb cylinder for the various MgF_2 strip thicknesses t . Here, the distance of propagation can be described as the distance that the domain of the field

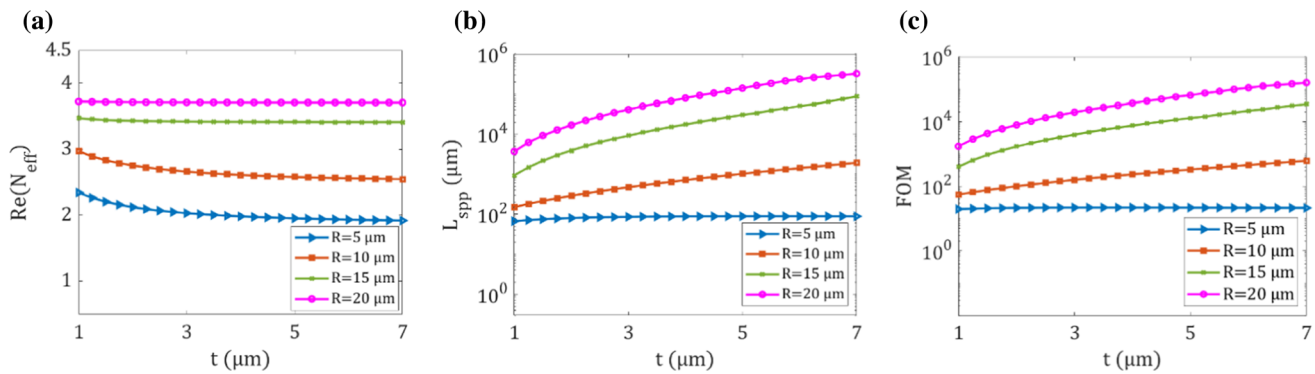


Fig. 8 Dependence of (a) the $\text{Re}(N_{\text{eff}})$, (b) L_{spp} and (c) FOM on MgF_2 strips thickness t for various radius R of the InSb cylinder

attenuates to $1/e$. For the fixed value of the MgF_2 strip thickness t , the propagation length, and figure of merit increase with the increasing radius R [see Fig. 7(b) and (c)]. In this case, the propagation length can be reached approximately as long as 10^5 micrometers. Therefore, the proper selection of the thickness t of MgF_2 strip and radius R of the InSb cylinder is resulted for obtaining the stronger confinement and longer propagation length.

Finally, we further demonstrate the efficacy of the cylinder radius (R) on the plasmonic features of the suggested structure as a function of the MgF_2 strip thickness t . Figure 8 shows that the proposed waveguide has got plasmonic properties that are strongly dependent on the thickness t of the MgF_2 strip and radius R of the InSb cylinder. Figure 8(a) shows that $\text{Re}(N_{\text{eff}})$ decrease with increasing the MgF_2 strip thickness t , for a lower radius (i.e., $R = 5$ μm and $R = 10$ μm), but the $\text{Re}(N_{\text{eff}})$ on MgF_2 strip thickness t just has a few changes for a higher radius (i.e., $R = 15$ μm and $R = 20$ μm). It can be observed that the L_{spp} and FOM of the proposed waveguide are dependent significantly on the cylinder radius R . [see Fig. 8(b) and 8(c)]. For example, for $R = 20$ μm , the L_{spp} drastically enhances on the strip thickness t from 3.71 mm at $t = 1$ μm to 342.5 mm at $t = 7$ μm . It can be seen that L_{spp} and FOM for InSb with higher cylinder radius (e.g., $R = 15$ μm and $R = 20$ μm) increase significantly as the strip thickness t increases. But, L_{spp} and FOM do not change approximately for the narrow cylinder (e.g., $R = 5$ μm).

For the fixed value of cylinder radius, L_{spp} and FOM increase by increasing the strip thickness t [see Fig. 8(b) and 8(c)]. Thus, for a certain InSb cylinder radius, the subwavelength strong confinement and long propagation length can be obtained by appropriate selection of the strip thickness.

4. Conclusions

In this study, we proposed a new GHPW structure including a high-index cylindrical dielectric in the coordinate origin, a low-index dielectric strip, and graphene layer surrounded by SiO_2 rectangular cube. We investigated the SPP propagation properties of GHPW in the far-infrared (FIR) domain. Results based on the simulation reveal that the GHPW could have a long propagation length and low propagation loss by tuning the dielectric material and geometry of the proposed waveguide in comparison with the similar waveguide structures. The most attractive property of the proposed waveguide is that via the selecting of appropriate materials for the low-index dielectric strip (MgF_2) with thickness of $t = 7$ μm and high-index dielectric cylinder (InSb) with the radius $R = 20$ μm , the ultralow propagation loss and high propagation distance (3.42×10^5 μm) can be obtained. Therefore, the proposed structure can contribute to the practical applications regarding the development of photonic devices at the far-infrared regime.

References

- [1] W L Barnes, A Dereux and T W Ebbesen *Opt. Nat.* **424** 824 (2003)
- [2] Y Qi, P Zhou, T Zhang, X Zhang, Y Wang, C Liu, Y Bai and X Wang *Results Phys.* **14** 102506 (2019)
- [3] J Chen, X Wang, F Tang, X Ye, L Yang and Y Zhang *Results Phys.* **16** 102867 (2020)
- [4] M B Heydari and M H V Samiei *Opt. Quantum Electron.* **52** 406 (2020)
- [5] Z Liu, G Liu, X Liu and G Fu *Nanotechnology* **31** 115208 (2019)
- [6] X Wang, Z Pang, H Yang and Y Qi *Results Phys.* **14** 102446 (2019)

- [7] M R Jafari, F Ebrahimi and M Nooshirvani *J. Appl. Phys.* **108** 054313 (2010)
- [8] M R Jafari and F Ebrahimi *J. Sci.* **21** 279 (2010)
- [9] M R Jafari and M Omid *Appl. Phys. A* **125** 466 (2019)
- [10] X He, T Ning, S Lu, J Zheng, J Li, R Li and L Pei *Opt. Express* **26** 10109 (2018)
- [11] D Teng et al. *Nanomaterials* **12** 1950 (2022)
- [12] N Ranjkesh, M Basha, A Taeb, A Zandieh, S Gigoyan and S Safavi-Naeini *IEEE Trans. THz Sci. Technol.* **5** 268 (2015)
- [13] T S Saini, A Kumar and R K Sinha *J. Light Wave Technol.* **33** 3914 (2015)
- [14] A S Hasan, R J Al-Azawi and A A Alwahib *Eng. Technol. J.* **40** 1 (2022)
- [15] E Moreno, S G Rodrigo and S I Bozhevolnyi *Rev. Lett.* **100** 023901 (2008)
- [16] H Gao, Q Cao, M Zhu, D Teng and S Shen *Opt. Express* **22** 32071 (2014)
- [17] Q Zhang, H Hao, J Ren, F Zhang, Q Gong and Y Gu *Nanoscale* **12** 10082 (2020)
- [18] R F Oulton, V J Sorger and D A Genov *Photonics* **2** 496 (2008)
- [19] Z Zhang and J Wang *Sci. Rep.* **4** 6870 (2014)
- [20] Y Gao, G Ren and B Zhu *Opt. Lett.* **39** 5909 (2014)
- [21] T J Huang, L Z Yin, J Zhao, C H Du and P K Liu *ACS Photon.* **7** 2173 (2020)
- [22] Y Gao and I V Shadrivov *Opt. Lett.* **41** 3623 (2016)
- [23] M R Jafari, B Bahrami and T Abolghasemi *J. Electron. Mater.* **46** 573 (2017)
- [24] R Aboltaman and M Shahmansouri *Commun. Theoret. Phys.* **72** 045501 (2020)
- [25] K S Novoselov, V I Fal, L Colombo, P R Gellert, M G Schwab and K Kim *Nature* **490** 192 (2012)
- [26] A K Giem and I V Grigorieva *Nature* **499** 419 (2013)
- [27] M B Heydari and M H V Samiei *Photon. Nanostruct. Fundamen. Appl.* **42** 100834 (2020)
- [28] K B M Rakib Hasan, M Asiful Islam and M Shah Alam *J. Opt. Soc. Am. B* **37** 2696 (2020)
- [29] M Dehghan, M K Moravvej-Farshi, M Ghaffari-Miab, M Jabbari and G Darvish *Plasmonics* **14** 1335 (2019)
- [30] M Shahmansouri and M Mahmodi Moghadam *Phys. Plasmas* **24** 102107 (2017)
- [31] M Mahmoudi Moghadam and M Shahmansouri *Phys. Scrip.* **95** 085606 (2020)
- [32] L Ye, K Sui, Y Liu, M Zhang and Q Liu *Opt. Express* **26** 15935 (2018)
- [33] M Heidari and V Ahmadi *IEEE Access* **7** 43406 (2019)
- [34] Z Yi et al. *Micromachines* **10** 194 (2019)
- [35] X Luo, Z Q Cheng, X Zhai, Z M Liu, S Q Li, J P Liu, L L Wang, Q Lin and Y H Zhou *Nanoscale Res. Lett.* **14** 1 (2019)
- [36] L Han, X He, L Ge, T Huang, H Ding and C Wu *Plasmonics* **14** 2021 (2019)
- [37] X He, T Ning, L Pei, J Zheng, J Li and J Wang *Results Phys.* **21** 103834 (2021)
- [38] Y Hajati, Z Zambouri and M Sabaeian *J. Opt. Soc. Am. B* **35** 446 (2018)
- [39] Y Sun, Y Bian, Z Zheng, J Liu and Z Gong *Photon. Conf. (IPC) IEEE* 544 (2013)
- [40] Y Sun Y Bian, X Zhao, Z Zheng, Jianwei Liu, and Jiansheng Liu *Opt. Soc. Am. JTU4A.33* (2013)
- [41] J Frigerio et al *Phys. Rev. B* **94** 085202 (2016)
- [42] J A Gonzalez-Cuevas, T F Refaat, M NurulAbedin and H E Elsayed-Ali *J. Appl. Phys.* **102** 014504 (2007)
- [43] D E Aspnes and A A Studna *Phys. Rev. B* **27** 985 (1983)
- [44] B O Seraphin and H E Bennett *Academic, New York* **3** 499 (1967)
- [45] M Saeed, A Ghaffar, S U Rehman, M Y Naz, S Shukrullah and Q A Naqvi *Plasmonics* **17** 901 (2022)
- [46] L Ye, Y Chen, G Cai, N Liu, J Zhu, Z Song and Q H Liu *Opt. Express* **25** 11223 (2017)
- [47] D Teng, Y Wang, T Xu, H Wang, Q Shao and Y Tang *Nanomaterials* **11** 1281 (2021)
- [48] G W Hanson *J. Appl. Phys.* **103** 064302 (2008)
- [49] W Zouaghi, D Voß, M Gorath, N Nicoloso and H G Roskos *Carbon* **94** 301 (2015)
- [50] A Asadi, M R Jafari and M Shahmansouri *Plasmonics* **17** 1819 (2022)

Publisher's Note Springer Nature remains neutral with regard to jurisdictional claims in published maps and institutional affiliations.

Springer Nature or its licensor (e.g. a society or other partner) holds exclusive rights to this article under a publishing agreement with the author(s) or other rightsholder(s); author self-archiving of the accepted manuscript version of this article is solely governed by the terms of such publishing agreement and applicable law.